Research on the contribution of s-process to the abundance of ^{94}Mo*

Chao Dong (董超)[1] Zhi-Hong Li (李志宏)[1,2,3†] Ge-Xing Li (李歌星)[1,3] Yun-Ju Li (李云居)[1] Na Song (宋娜)[1]
Chen Chen (陈晨)[1] Jun-Wen Tian (田竣文)[1] Jia-Ying-Hao Li (李家英豪)[1] Zhi-Cheng Zhang (张智程)[1]
Hui-Ling Tian (田慧玲)[1] Mei-Yue-Nan Ma (马梅月楠)[1]

[1]China Institute of Atomic Energy, Beijing 102413, China
[2]University of Chinese Academy of Sciences, Beijing 101408, China
[3]Jinping Deep Underground Frontier Science and Dark Matter Key Laboratory of Sichuan Province, Liangshan 615000, China

Abstract: This paper addresses a long-standing problem in astrophysics—the origin of the solar system abundance of the proton-rich isotope ^{94}Mo by proposing a valuable novel mechanism. The main contribution of this work is that it challenges the traditional view of "^{94}Mo as a pure p-process nuclide". For the first time, it demonstrates that within the s-process environment of low-mass AGB stars, a new s-process path (^{93}Zr → ^{93}Nb →^{94} Nb →^{94} Mo) for producing ^{94}Mo can be opened, enabled by the significant enhancement of the effective decay rates of ^{93}Zr and ^{94}Nb due to the high-temperature astrophysical environment. The results show that this s-process channel can contribute up to a maximum of approximately 10.6% to the solar system abundance of ^{94}Mo. This work provides a new s-process perspective on the origin of ^{94}Mo and has implications for reevaluating the sources of other "shielded" p-nuclei.

Keywords: stellar nucleosynthesis, ^{94}Mo, effective decay rate, AGB stars

DOI: 10.1088/1674-1137/ae5ef4 **CSTR:** 32044.14.ChinesePhysicsC.50074102

I. INTRODUCTION

The production of elements heavier than iron primarily occurs through neutron capture processes: a slow neutron capture process (s-process) and a rapid neutron capture process (r-process) [1]. However, 35 proton-rich stable isotopes (p-nuclei) are bypassed by these processes owing to their neutron-deficient nature [2]. Notably, most p-nuclei are approximately 2 orders of magnitude less abundant than other stable isotopes in the same isotope chain, except for the isotopes ^{92,94}Mo and ^{96,98}Ru [2]. Their synthesis in stars remains a major unsolved problem in nuclear astrophysics, as current models underproduce their abundances by several orders of magnitude [3]. The standard paradigm for their origin is the γ-process (or p-process), which takes place in the O/Ne-rich layers of massive stars during their explosion as Type II supernovae (SNe II) [4–8]. While the γ-process successfully accounts for the bulk of the p-nuclides, a long-standing and well-documented problem exists: it significantly underproduces the solar abundances of certain p-nuclei, most notably isotopes ^{92}Mo and ^{94}Mo [2, 4, 7, 8].

To address this deficiency, several alternatives or additional production mechanisms have been proposed. The neutrino-proton process (νp-process), occurring in the proton-rich neutrino-driven winds of core-collapse supernovae, has been identified as a promising candidate [9]. In this process, antineutrino absorption on protons provides a source of free neutrons that can bypass slow β^+-decays, enabling the synthesis of nuclei beyond A=64 and potentially accounting for the solar abundances of ^{92,94}Mo and ^{96,98}Ru [9]. However, the viability of the νp-process has recently been challenged by nuclear physics considerations. Jin *et al.* [10] suggested that particle-induced de-excitation of the Hoyle state in ^{12}C could significantly enhance the triple-α reaction rate, leading to increased production of seed nuclei that would suppress the νp-process flow towards heavier elements. Fortunately, a recent groundbreaking experiment by Bishop *et al*. [11] directly measured the cross section for neutron-induced inelastic scattering to the Hoyle state, finding it to be much smaller than previously predicted by Hauser-Feshbach calculations. This implies that neutron-induced de-excitation of the Hoyle state has a negligible effect on the triple-α rate and, consequently, on the νp-process. A subsequent theoretical study by Sasaki *et al.* [12] incorporated these new experimental constraints and found that,

Received 6 February 2026; Accepted 13 April 2026; Accepted manuscript online 14 April 2026

* This work was supported by the National Natural Science Foundation of China (12475151, 12405164), the Continuous-Support Basic Scientific Research Project (BJ010261223284)

† E-mail: zhli@ciae.ac.cn

while proton-induced de-excitation still suppresses the *v*p-process in ordinary supernova winds, it is alleviated in the high-entropy winds of hypernovae, where the *v*p-process can remain a robust source of Mo and Ru [12, 13]. Despite these advances, the *v*p-process remains subject to significant uncertainties, including the detailed properties of neutrino-driven winds [14] and the effects of collective neutrino oscillations [15, 16].

Song *et al*. [17] employed the Gross Theory of Beta Decay (GTBD) model and supernova explosion simulations to calculate the contribution of neutrino-induced reactions to the nucleosynthesis of ^{94}Mo, providing important quantitative constraints on the astrophysical origin of this isotope. This study provided a new perspective on the origin of p-process nuclei in the solar system [17]. Their calculations show that the neutrino process can account for up to approximately 6.8% of the solar system abundance of ^{94}Mo [17]. However, the study also reveals that neutrino-nucleus reactions are not the dominant production channel for ^{94}Mo, implying that a significant fraction of its origin remains unexplained by current mechanisms. Therefore, the complete nucleosynthetic picture of ^{94}Mo remains unclear, calling for further exploration of other possible astrophysical sites or reaction mechanisms.

The p-process has abundances approximately 2 orders of magnitude lower than those produced by the s-process and r-process [17]. Therefore, the origin of relatively abundant p-nuclei such as ^{94}Mo may require a re-evaluation of potential contributions from the s-process. Fig. 1 shows the s-process path near ^{94}Mo. The conventional view holds that at the s-process branching point, the half-life of the key nuclide ^{93}Zr (the ground state, $t_{1/2} = 1.61\times10^{6}$ years [18]) is much longer than the typical s-process timescale. Consequently, ^{93}Zr is considered essentially stable in the s-process environment, undergoing negligible β^--decay to ^{93}Nb, which leads to the dismissal of the s-process as a contributor to ^{94}Mo. However, this deduction overlooks the influence of the astrophysical environment on the decay rate. A certain probability remains that nuclei will be excited to a low-excited state by high-energy photons in the astrophysical environment. However, the first excited state of ^{93}Zr (at 266.88 keV) has a relatively low log ft value (approximately 8.4 [19]) and a much shorter half-life (approximately 20 years). This half-life is comparable to the s-process timescale, implying that at sufficiently high temperatures, thermal population of excited states can significantly enhance the β^--decay branching ratio of ^{93}Zr via this excited state. Thus, in a hot s-process environment, ^{93}Zr may effectively decay to ^{93}Nb. Subsequently, ^{93}Nb can capture a neutron to form ^{94}Nb. The terrestrial half-life of ^{94}Nb is $t_{1/2} = 2\times10^{4}$ y; however, at $T = 3\times10^{8}$ K, it drops to 9.3 days [19]. Finally, ^{94}Nb undergoes β^--decay to produce stable ^{94}Mo. This opens up a new generation path for ^{94}Mo elements, as indicated by the blue arrow in Fig. 1.

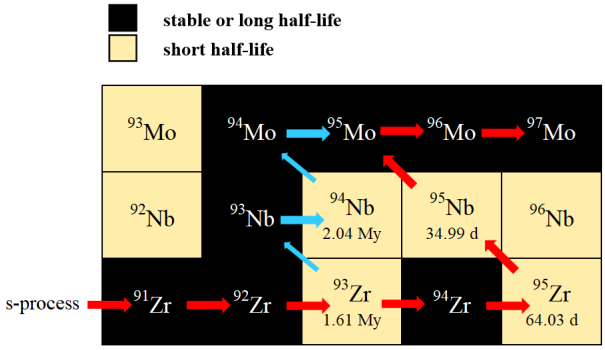

Fig. 1. (color online) S-process path in the region of ^{94}Mo.

In this study, we investigated a previously overlooked s-process channel for ^{94}Mo production in detail. This channel proceeds via the thermally enhanced β^--decay of ^{93}Zr followed by neutron capture. We quantitatively calculated the potential contribution of this channel to the ^{94}Mo abundance under temperature and neutron flux conditions of various s-process astrophysical sites. This study not only provides a new perspective for understanding the origin of ^{94}Mo but may also be significant for re-evaluating the s-process origins of other "shielded" p-nuclei.

II. METHODOLOGY

Key nuclide ^{93}Zr is the starting point of our proposed mechanism. The complete reaction path under consideration is ^{93}Zr$(\beta^-)^{93}$Nb$(n,\gamma)^{94}$Nb$(\beta^-)^{94}$Mo. Its primary astrophysical source is found in the chemical evolution of a galaxy within low-mass (approximately 1.5–3 $M_\odot$) AGB stars. Iben *et al*. [20, 21] established the classical framework for understanding nucleosynthesis during the thermally-pulsing AGB phase of low-mass stars. This model drives s-process nucleosynthesis through convective motions within the helium-burning shell during thermal pulses. During a thermal pulse, nucleosynthesis occurs within the helium-burning shell, and neutron sources are activated [20]. These neutrons are captured by iron seed nuclei, synthesizing heavy elements via the slow neutron-capture process (s-process) [20]. After the pulse ends, a long interpulse phase begins, during which there is no active neutron source in the shells [20]. Therefore, s-process nucleosynthesis occurs only during the brief thermal pulses, not throughout the entire AGB stars phase. This cycle of "burning during pulses and dormancy during interpulse phases" constitutes the fundamental characteristic of periodic nucleosynthesis in the AGB stars phase [20]. Our calculations to track the s-process nucleosynthetic flow through the ^{93}Zr branching point were built upon a Pulsed Irradiation Model (PIM) [22, 23], which captures this essential cyclic behavior. A key assumption in our application of this model is the

treatment of physical parameters: the pulse and interpulse durations (t_p, t_{ip}), pulse and interpulse temperatures (T_p, T_{ip}), electron number densities (N_e), and neutron density during pulses (N_n) are held constant from one cycle to the next [22, 23]. According to the typical conditions in AGB stars, ranges for these representative parameters are as follows: $N_n = 10^7 \sim 10^8$ cm^{-3}, $N_e = 3\times10^{26} \sim 3\times10^{27}$ cm^{-3} [22, 23].

In this established framework, the synthesis and evolution of specific s-process nuclides, such as ^{93}Zr, are governed by the cyclical alternation between thermal pulses and interpulse. During a thermal pulse, the activated neutron source provides a sustained neutron flux. Seed nuclei capture neutrons successively along the valley of β-stability [20–23]. At this stage, the abundance of ^{93}Zr varies with time as

$$\frac{\mathrm{d}N(^{93}\mathrm{Zr})}{\mathrm{d}t} = N(^{92}\mathrm{Zr}) < \sigma_{^{92}\mathrm{Zr}} v > N_n - N(^{93}\mathrm{Zr}) < \sigma_{^{93}\mathrm{Zr}} v > N_n - N(^{93}\mathrm{Zr})\lambda^{\beta}_{^{93}\mathrm{Zr}}, \quad (1)$$

where N is the abundance, N_n is the abundance of neutron, σ is the neutron capture cross section, v is the relative velocity of neutrons and a target nuclide, $\langle\sigma v\rangle$ is the reaction rate of each pair of nuclei, and $\lambda^{\beta}_{^{93}\mathrm{Zr}}$ is the β^- decay rate of ^{93}Zr. This intense neutron-capture phase exhibits a relatively short duration, typically on the order of a hundred years. When the neutron radiation reaches sufficient intensity —specifically, by the end of each pulse—a state of local equilibrium is established. In this state, the abundance of an s-process nuclide is inversely proportional to its neutron capture reaction rate $\langle\sigma v\rangle$, defining the local equilibrium [24]. That is, at the end of each pulse, the abundance ratio of ^{93}Zr to ^{92}Zr equals the inverse ratio of their neutron-capture cross-sections,

$$\frac{N(^{93}\mathrm{Zr})}{N(^{92}\mathrm{Zr})} = \frac{\langle\sigma_{^{92}\mathrm{Zr}} v\rangle}{\langle\sigma_{^{93}\mathrm{Zr}} v\rangle}. \quad (2)$$

Subsequently, the star enters a long interpulse period lasting approximately 10^4–10^5 years [22, 23]. Without neutron irradiation, unstable ^{93}Zr produced in the preceding pulse undergoes β^- decay to stable ^{93}Nb. This decay-dominated phase significantly alters the isotopic inventory, reducing the abundance of ^{93}Zr while accumulating its decay daughter ^{93}Nb. At this stage, the abundance of ^{93}Nb varies with time as

$$\frac{\mathrm{d}N(^{93}\mathrm{Nb})}{\mathrm{d}t} = N(^{93}\mathrm{Zr})\lambda^{\beta}_{^{93}\mathrm{Zr}}, \quad (3)$$

and when the next thermal pulse is triggered, the neutron flux resumes [22, 23]. Note that ^{93}Nb accumulated during the interpulse now acts as a new seed nucleus. It captures a neutron to form ^{94}Nb, which then decays via β^- to produce ^{94}Mo. At this stage, the abundance of ^{94}Nb and ^{94}Mo varies with time as

$$\frac{\mathrm{d}N(^{94}\mathrm{Nb})}{\mathrm{d}t} = N(^{93}\mathrm{Nb})\langle\sigma_{^{93}\mathrm{Nb}} v\rangle N_n - N(^{94}\mathrm{Nb})\langle\sigma_{^{94}\mathrm{Nb}} v\rangle N_n - N(^{94}\mathrm{Nb})\lambda^{\beta}_{^{94}\mathrm{Nb}}, \quad (4)$$

$$\frac{\mathrm{d}N(^{94}\mathrm{Mo})}{\mathrm{d}t} = N(^{94}\mathrm{Nb})\lambda^{\beta}_{^{94}\mathrm{Nb}} - N_{^{94}\mathrm{Mo}}\langle\sigma_{^{94}\mathrm{Mo}} v\rangle N_n. \quad (5)$$

This exemplifies how the s-process advances through iterative cycles: neutron capture during pulses builds nuclei up the mass chain, while β-decay during interpulses reshapes the isotopic composition, preparing nuclei for further neutron capture in subsequent pulses.

Following the framework of PIM, the final abundance ratio $N(^{94}\mathrm{Mo})/N(^{92}\mathrm{Zr})$ is obtained by iterating the differential equations (Eqs.(2)–(5)) through successive pulse-interpulse cycles.

III. INPUT PHYSICS

Pioneering work by Cameron [25] demonstrated the importance of thermally populated nuclear excited states in enhancing decay rates. In particular, nuclei are frequently excited by high-energy photons in stellar environments, leading to decay rates that differ significantly from those of ground states. Moreover, Bahcall [26] and Peterson and Bahcall [27] concluded that an elevated electron number density enhances the electron-capture (EC) rates by supplying more high-energy electrons while simultaneously suppressing the β^- decay through Pauli blocking (occupied final electron states) [28]. Temperatures and densities can vary greatly in different nucleosynthesis environments. Effective decay rate was first shown in the seminal work by Takahashi and Yokoi published in 1987 [19]. Under this framework, the effective β^- decay rate of nuclei in the astrophysical environment is

$$\lambda = \sum_l P_l \sum_k P_k \lambda_{l,k}, \quad (6)$$

where the subscript k is k-times ionized and the subscript l is the nuclear level. Note that P_l is the population probability at thermal equilibrium whereas P_k is the probability of ion; λ is the decay rate and $\lambda_{l,k}$ is [29]

$$\lambda_{l,k} = \frac{\ln 2}{ft}\int_1^{Q_{ij}} W\sqrt{W^2-1}(Q_{ij}-W)^2 F_0(Z+1,W) S_m(Z+1,W)(1-G_e(W))(1-G_\nu(Q_{ij}-W))\mathrm{d}W, \quad (7)$$

where ft is the comparative half-life. W is the total energy of the electron or positron, both rest mass and kinetic, in units of m_ec^2. Z is the proton number of parent nucleus. Q_{ij} is the decay energy between the initial state of the parent i and the final state of the daughter j in units of m_ec^2. $W_{\rm min}$ is the lowest energy of the electron(positron) in the β^--decay in units of m_ec^2. $F(Z,W)$ is the Fermi function [30–33]. $S_m(Z,W)$ denotes the spectral shape factors [31, 32, 34].

The seminal work by Takahashi and Yokoi published in 1987 [19] provided a foundational framework and extensive datasets for calculating effective decay rates in stellar environments, which have been widely adopted as a primary reference in astrophysical network computations. In this study, the latest evaluated log ft values from the National Nuclear Data Center (NNDC) were employed as key input parameters for calculating the effective decay rates of ^{93}Zr and ^{94}Nb, as listed in Tables 1 and 2.

As clearly shown in Fig. 2 and Fig. 3, the effective β^--decay rates of both ^{93}Zr and ^{94}Nb exhibit a strong dependence on temperature. Furthermore, in the astrophysical environment of interest, the effective decay rate of ^{94}Nb is not as sensitive to the electron density as that of ^{93}Zr. At the temperature of interest $T = 3\ T_8$, the effective decay rate of ^{93}Zr is 5.51×10^{-14} s^{-1}, and its half-life is 0.40 My, which is 40 times shorter than the value of 16.1 My measured in the laboratory. The effective decay rate of ^{94}Nb is 9.49×10^{-7} s^{-1} and its half-life is 8.45 d, which is 8.80×10^{7} times shorter than the value of 2.04 My measured in the laboratory. These values dramatically enhanced the mean of decay rates such that under astrophysical conditions, the β^--branching of the s-process at ^{94}Nb and ^{93}Zr in AGB stars is increased, thereby redirecting the flow toward ^{94}Mo.

In this study, the neutron-capture rates required as input for our nucleosynthesis network calculations were computed following the formalism presented by Pritychenko [36]. The reaction rates were derived from the evaluated nuclear data library ENDF/B-VIII.0 [37], which provides a complete collection of neutron-induced cross sections over the energy range 10^{-5} eV−20 MeV [36]. The calculations covered the temperature interval 0.01–10 GK, corresponding to the typical range of slow-neutron capture (s-process) nucleosynthesis [36]. To facilitate the implementation in our reaction network, the calculated rates were parameterized in the standard REACLIB format [38] using the seven-term expression [36]. The neutron capture reaction rate of ^{92}Zr,^{93}Zr,^{93}Nb,^{94}Nb, and ^{94}Mo is shown in Fig. 4. The correlation between the neutron capture rates of these elements and temperature is evident.

Table 1. Log ft values for the decay of ^{93}Zr → ^{93}Nb [18].

Transitions	Log ft
g.s.→g.s.	12.10
g.s.→0.03082 MeV	10.17
0.26688 MeV→0.03082 MeV	8.40

Table 2. Log ft values for the decay of ^{94}Nb → ^{94}Mo [35].

g.s.→1.57372 MeV	11.95
0.040892 MeV→0.871087 MeV	6.50
0.040892 MeV→1.57372 MeV	7.34
0.040892 MeV→1.86427 MeV	6.76
0.058708 MeV→1.57372 MeV	6.50
0.1134009 MeV→1.57372 MeV	6.50
0.140298 MeV→g.s.	9.50
0.140298 MeV→0.871087 MeV	7.50
0.140298 MeV→1.86427 MeV	6.50

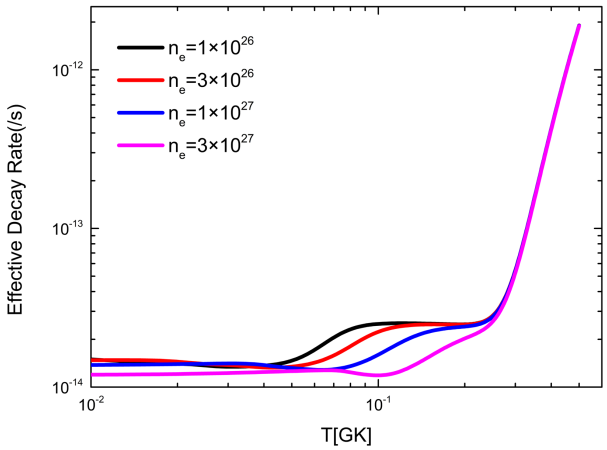

Fig. 2. (color online) Effective decay rate of ^{93}Zr as a function of temperature and electron number density.

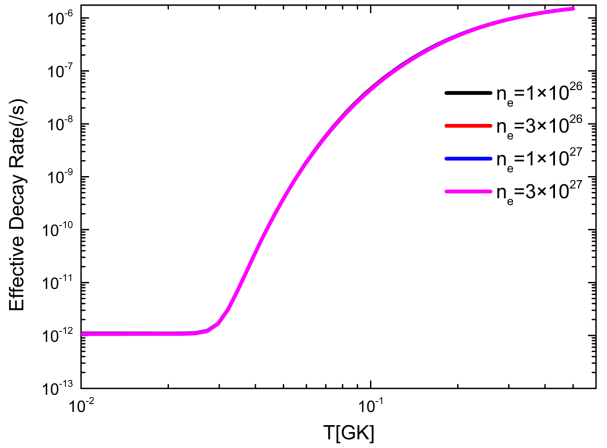

Fig. 3. (color online) Effective decay rate of ^{94}Nb as a function of temperature and electron number density.

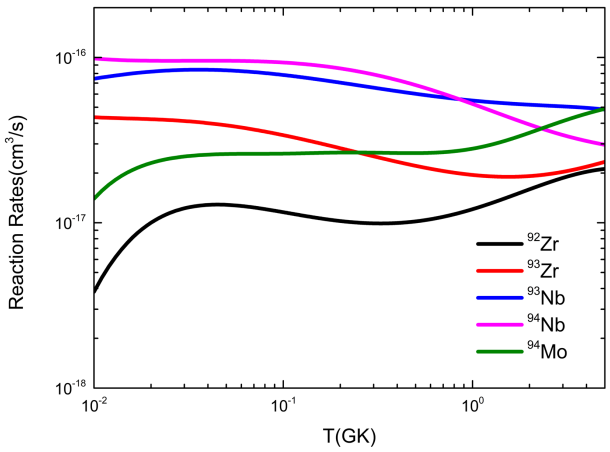

Fig. 4. (color online) Neutron capture reaction rate of ^{92}Zr, ^{93}Zr, ^{93}Nb, ^{94}Nb, and ^{94}Mo as a function of temperature.

IV. CONTRIBUTION OF THE S-PROCESS TO THE ABUNDANCE OF ^{94}Mo

Karakas *et al*. [39, 40] conducted systematic evolutionary simulations of low- and intermediate-mass AGB stars, providing detailed structural parameters from the zero-age main sequence to the end of the thermal pulse (TP) phase. These include core mass ($M_{\rm core}$), maximum helium shell temperature ($T_{\rm Heshell}$), maximum temperature at the base of the convective envelope during the previous interpulse period ($T_{\rm bce}$), hydrogen shell temperature ($T_{\rm Hshell}$), duration of intershell convection, and $t_{\rm csh}$ and interpulse period (*interpulse*) for various masses (1–6 $M_{\odot}$) and metallicities (Z=0.02–0.0001). These models provide essential input parameters for subsequent studies on AGB stellar nucleosynthesis, mass loss, and chemical element yields.

To quantify the s-process production of ^{94}Mo, we mapped the stellar structure parameters from Karakas *et al.* [39, 40] into the (PIM) framework [22, 23]. Specifically, $T_{\rm Heshell}$ and $T_{\rm Hshell}$ informed our choices for the pulse temperature $T_{\rm p}$ and interpulse temperature $T_{\rm ip}$, and $t_{\rm csh}$ and *interpulse* informed our choices for the pulse and interpulse durations $t_{\rm p}$ and $t_{\rm ip}$. The neutron density N_n and electron density N_e were explored over the ranges $N_n = 10^7 \sim 10^8$ cm^{-3}, $N_e = 3\times10^{26} \sim 3\times10^{27}$ cm^{-3}, respectively, covering conditions relevant to the s-process in AGB stars [22, 23]. By iteratively solving the set of equations defined by Eqs.(2)–(5) through successive pulse-interpulse cycles within this framework, we obtained the final abundance ratio $N(^{94}\text{Mo})/N(^{92}\text{Zr})$. The results for selected stellar masses and metallicities are summarized in Table 3.

A key feature of our calculations is the explicit inclusion of stellar environmental effects on the nuclear rates. The β^--decay rates of ^{93}Zr and ^{94}Nb are taken as their temperature- and density-dependent effective values (Sec. III) and the neutron-capture rates (n, γ) are temperature-dependent (Sec. III). This ensures that the influence of the hot AGB star interior on the entire reaction flow ^{93}Zr $\rightarrow$ ^{93}Nb $\rightarrow^{94}$ Nb $\rightarrow^{94}$ Mo is fully accounted for.

The calculated yield ratios $N(^{94}\text{Mo})/N(^{92}\text{Zr})$ in Table 3 reveal a clear correlation with the neutron and electron number densities. For a given stellar model, a lower neutron density (*e.g.*, $N_n = 10^7$, Cases A & B) systematically leads to a higher production ratio compared to the cases with a higher neutron density (*e.g.*, $N_n = 10^8$, Cases C & D). Similarly, for a fixed neutron density, a lower electron number density (*e.g.*, $N_e = 3\times10^{26}$ cm^{-3}, Cases A & C) generally yields a larger value than its counterpart with a higher electron density (*e.g.*, $N_e = 3\times10^{27}$ cm^{-3}, Cases B & D). Under conditions of lower neutron and electron densities, the β^--decay branch of $N(^{93}\text{Zr})$ within the s-process is enhanced, leading to increased production of $N(^{93}\text{Nb})$ as seed nuclei. Meanwhile, given that the total number of seed nuclei per pulse is finite, a lower

Table 3. Calculated yield ratio ^{94}Mo from the s-process under different AGB stars model parameters.

Parameter of AGB stars		Yield ratio ($N(^{94}\text{Mo})/N(^{92}\text{Zr})$)			
Mass ($M_{\odot}$)	Metallicitiy (Z)	Case A $N_n = 10^7$ $N_e = 3\times10^{26}$	Case B $N_n = 10^7$ $N_e = 3\times10^{27}$	Case C $N_n = 10^8$ $N_e = 3\times10^{26}$	Case D $N_n = 10^8$ $N_e = 3\times10^{27}$
3.0	0.0001	1.21×10^{-2}	8.60×10^{-3}	1.47×10^{-4}	1.06×10^{-4}
3.0	0.004	1.27×10^{-2}	1.02×10^{-2}	2.37×10^{-6}	1.90×10^{-6}
3.0	0.008	7.42×10^{-3}	7.38×10^{-3}	3.98×10^{-3}	3.30×10^{-3}
2.1	0.008	4.33×10^{-3}	4.15×10^{-3}	1.28×10^{-9}	1.11×10^{-9}
2.0	0.0001	6.67×10^{-3}	3.75×10^{-3}	5.13×10^{-7}	4.36×10^{-7}
1.9	0.004	6.71×10^{-3}	5.67×10^{-3}	5.53×10^{-9}	4.79×10^{-9}
1.5	0.0001	6.57×10^{-3}	5.82×10^{-3}	7.93×10^{-8}	6.90×10^{-8}
1.5	0.004	5.42×10^{-3}	4.76×10^{-3}	9.16×10^{-11}	8.03×10^{-10}
1.5	0.008	8.10×10^{-3}	7.10×10^{-3}	1.13×10^{-8}	9.90×10^{-9}

neutron density limits the advancement of the neutron-capture chain towards heavier nuclei, thereby causing more nucleosynthetic flow to accumulate around ^{94}Mo. By comparing the results of AGB stars with different masses and metallicities, we found that the yield of ^{94}Mo is primarily influenced by the durations of the thermal pulses and the interpulse periods. Specifically, a longer duration of the interpulse allows more time for the β^- decay of ^{93}Zr, thereby accumulating more ^{93}Nb as seed nuclei for the next pulse. Conversely, a shorter pulse duration limits the progression of the neutron-capture chain to heavier nuclei, favoring the accumulation of the nucleosynthetic flow at ^{94}Mo. Therefore, the most efficient production of ^{94}Mo via the ^{93}Zr branching occurs under conditions of concurrently low neutron, low electron densities, and with a pulse-interpulse cycle characterized by a long interpulse and a short pulse duration.

Compared to the early solar system abundance ratio of $N(^{94}\mathrm{Mo})/N(^{92}\mathrm{Zr}) \approx 0.12$, our calculated maximum yield ratio from this s-process channel reaches approximately 1.27×10^{-2} (see Table 3, Case A for the 3.0 $M_\odot$, Z=0.0001 model). This corresponds to a maximum relative contribution of approximately 10.6% of the solar system abundance of $N(^{94}\mathrm{Mo})$ that could originate from the s-process in low-mass AGB stars. To evaluate the impact of uncertainties in key nuclear reaction rates on the results, we performed an error analysis. Specifically, we varied the neutron capture cross sections and β-decay rates by ±10%. The simulations indicate that this ±10% variation in reaction rates translates to a ±3% (absolute) uncertainty in the estimated contribution.

It is important to note that Eqs. (2)−(5) constitute a highly simplified, localized network focused on the most direct path in the Zr-Nb-Mo region. While this approach successfully captures the essential physics of the proposed ^{93}Zr branching mechanism and provides a crucial first quantitative estimate of its potential contribution, it does not encompass the full complexity of the s-process in AGB stars. In reality, the s-process flow in this mass region is influenced by additional branching points (*e.g.*, at ^{95}Zr ^{95}Mo) and competing reactions. Therefore, our current yield ratio $N(^{94}\mathrm{Mo})/N(^{92}\mathrm{Zr})$ should be viewed as an evaluation within this focused framework. To obtain more precise quantitative results, future work necessitates embedding this branching study into a complete s-process reaction network covering a broader mass range. This will allow for a comprehensive assessment of how other potential branchings might affect the final yield of ^{94}Mo.

V. SUMMARY

In this study, we propose a new approach to reassessing the astrophysical origin of "shielded" p-nuclei: in high-temperature stellar environments, the β^--decay rates of key nuclides can be significantly enhanced owing to thermal excitation, thereby opening new branches in the traditional s-process path and allowing some p-nuclei to be synthesized via the s-process. This mechanism is not only applicable to explaining the origin of ^{94}Mo but also provides a new theoretical perspective for understanding the origin of other similar p-nuclei.

For ^{94}Mo, we propose for the first time that a new s-process path via ^{93}Zr $\rightarrow^{93}$ Nb $\rightarrow$ ^{94}Nb $\rightarrow^{94}$ Mo in low-mass AGB stars can contribute to its solar system abundance. Calculations show that this channel can contribute up to approximately 10.6% of the total solar system abundance of ^{94}Mo (which has an isotopic fraction of 9.15% relative to all Mo isotopes [41]). Its production efficiency is mainly regulated by three factors: 1) Electron density: Lower electron density favors the β^--decay branching of ^{93}Zr; 2) Neutron density: Lower neutron density suppresses the advancement of the neutron-capture chain toward heavier nuclei, allowing more nucleosynthetic flow to accumulate at ^{94}Mo; 3) Pulse duration: Shorter pulse duration likewise restricts the neutron-capture process. Under the above conditions, the nucleosynthetic flow can accumulate more effectively around ^{94}Mo. Simultaneously, longer interpulse periods provide more sufficient time for the decay of ^{93}Zr, thereby accumulating more ^{93}Nb as seed nuclei. Integrating the above factors, the internal environments of AGB stars conducive to the efficient production of ^{94}Mo via this mechanism should exhibit the following characteristics: relatively low electron density, low neutron density, short pulse duration, and long interpulse periods.

In contrast with the s-process abundance decomposition for Mo isotopes reported by Bisterzo *et al.* [42, 43], who derived an s-process contribution of 0.9% for ^{94}Mo, this study raises the s-process contribution of the solar system abundance of ^{94}Mo to 10.6%, a significant upward revision. This mechanism may also have a limited impact on other Mo isotopes. For instance, using the same methodological framework as applied to ^{94}Mo, we obtain that the enhanced decay of ^{94}Nb could increase the s-process contribution to ^{95}Mo by up to 1.9%.

Future work should extend this study by exploring a broader parameter space of AGB stars, performing more accurate network calculations, and conducting a comprehensive analysis of the combined contributions from other nucleosynthetic processes.

References

[1] E. M. Burbidge, G. R. Burbidge, W. A. Fowler *et al*., Rev. Mod. Phys. **29**, 547 (1957)
[2] M. Arnould and S. Goriely, Phys. Rep **384**, 1 (2003)
[3] K. Göbel, J. Glorius, A. Koloczek *et al*., EPJ Web Conf. **93**, 03006 (2015)
[4] T. Sauter and F. Käppeler, Phys. Rev. C **55**, 3127 (1997)
[5] M. Arnould, A & A **46**, 117 (1976)
[6] S. E. Woosley and W. M. Howard, Astrophys. J. Suppl. Ser **36**, 285 (1978)
[7] M. Rayet, M. Arnould, M. Hashimoto *et al*., A & A **298**, 517 (1995)
[8] T. Rauscher, A. Heger, R. D. Hoffman *et al*., ApJ **576**, 323 (2002)
[9] C. Fröhlich, G. Martínez-Pinedo, M. Liebendörfer *et al*., Phys. Rev. Lett. **96**, 142502 (2006)
[10] S. Jin, L. F. Roberts, S. M. Austin *et al*., Nature **588**, 57 (2020)
[11] J. Bishop, C. E. Parker, G. V. Rogachev *et al*., Nat. Commun. **13**, 2151 (2022)
[12] H. Sasaki, Y. Yamazaki, T. Kajino *et al*., Phys. Lett. B **851**, 138581 (2024)
[13] H. Sasaki, Y. Yamazaki, T. Kajino *et al*., ApJ **924**, 29 (2022)
[14] N. N. Weinberg, L. Bildsten and H. Schatz, ApJ **639**, 1018 (2006)
[15] H. Sasaki, T. Kajino, T. Takiwaki *et al*., Phys. Rev. D **96**, 043013 (2017)
[16] X. Yao, T. Kajino, Y. Luo *et al*., ApJ **980**, 247 (2025)
[17] N. Song, Z. H. Li, G. X. Li *et al*., ApJ **990**, 11 (2025)
[18] C. M. Baglin, Nucl. Data Sheets **112**, 1163 (2011)
[19] K. Takahashi and K. Yokoi, At. Data Nucl. Data Tables **36**, 375 (1987)
[20] I. Iben and A. Renzini, Annu. Rev. Astron. Astrophys. **21**, 271 (1983)
[21] I. Iben, ApJ. **196**, 525 (1975)
[22] K. Yokoi, K. Takahashi and M. Arnould, A & A **145**, 339 (1985)
[23] M. Arnould, K. Takahashi and K. Yokoi, A & A **137**, 51 (1984)
[24] B. Pritychenko, S. F. Mughaghab and A. A. Sonzogni, At. Data Nucl. Data Tables **96**, 645 (2010)
[25] A. G. W. Cameron, ApJ. **130**, 452 (1959)
[26] J. N. Bahcall, ApJ. **139**, 318 (1964)
[27] V. L. Peterson and J. N. Bahcall, ApJ. **138**, 437 (1963)
[28] G. M. Fuller, W. A. Fowler and M. J. Newman, Astrophys. J. Suppl. Ser **42**, 447 (1980)
[29] C. Dong, Z. H. Li, G. X. Li *et al*., Chin. Phys. C **49**, 094110 (2025)
[30] K. Langanke and G. Martínez-Pinedo, Nucl. Phys. A **673**, 481 (2000)
[31] E. J. Konopinski and G. E. Uhlenbeck, Phys. Rev. **60**, 308 (1941)
[32] J. P. Davidson, Phys. Rev. **82**, 48 (1951)
[33] K. Takahashi and K. Yokoi, Nucl. Phys. A **404**, 578 (1983)
[34] S. Liu and C. Xu, Chin. Phys. C **46**, 054106 (2022)
[35] D. Abriola and A. A. Sonzogni, Nuclear Data Sheets **107**, 2423 (2006)
[36] B. Pritychenko, Nucl. Data Sheets **167**, 76 (2020)
[37] D. A. Brown, M. B. Chadwick, R. Capote *et al*., Nucl. Data Sheets **148**, 1 (2018)
[38] R. H. Cyburt, A. M. Amthor, R. Ferguson *et al*., Astrophys. J. Suppl. Ser **189**, 240 (2010)
[39] A. I. Karakas, Mon. Not. R., Astron. Soc. **403**, 1413 (2010)
[40] A. I. Karakas and J. C. Lattanzio, Publ. Astron. Soc. Aust. **24**, 103 (2007)
[41] K. Lodders, ApJ **591**, 1220 (2003)
[42] S. Bisterzo, R. Gallino, O. Straniero *et al*., MNRAS **418**, 284 (2011)
[43] S. Bisterzo, C. Travaglio, R. Gallino *et al*., ApJ **787**, 10 (2014)